Heat Transfer Engineering, 31(2):101–107, 2010

ISSN: 0145-7632 print / 1521-0537 online
DOI: 10.1080/01457630903285302

Taylor & Francis
Taylor & Francis Group

Electrowetting Purged Surface Condensate in Evaporators

JEDO KIM and MASSOUD KAVIANY
Department of Mechanical Engineering, University of Michigan, Ann Arbor, Michigan, USA

Condensate electrowetting purge in evaporators (heat exchangers) based on the force balance at the three-phase contact line (TCL) is used in a prototype heat exchanger. The electrowetting is described based on overcoming the static three-phase contact line friction and detailed droplet physics is presented. Series of experiments was performed under various conditions and it was found that electrowetting combined with hydrophobic coating improves the drainage rate by as much as factor of three. Observations show that fins subjected to electrowetting are cleared of liquid droplets, in contrast to the fins which are not. Based on the proposed physics and experimental data, optimized electrode designs for future reference are proposed.

INTRODUCTION

Dropwise condensation occurs when moist air flows in refrigeration or air-conditioning evaporators, and can block the air passage and degrade the performance, thus requiring periodic water surface droplet or frost purging (Emery and Siegel [1], Na and Webb [2], and Ren et al. [3]). Surface modifications have been devised to reduce the critical angle at which a given volume surface droplet begins to slide under gravity. These include the recent study by Adamson [4], who achieved a 50% reduction in the volume needed for the onset of droplet sliding, using a micro-grooved (directional) aluminum surface. However, these passive surface modification techniques are not suitable for versatile operating conditions and active control of the condensate. We examine theoretical and experimental aspects of purging surface droplets by electrowetting, a phenomenon based on the interaction of the electrostatic, gravity and surface forces. In analyzing the electrowetting process a detailed description of the dynamics at the three-phase contact line (TCL) is required. However, the classical hydrodynamics cannot fully describe the motion of the TCL. Several strategies have been introduced to resolve the problem (deGennes [5], Oron [6], and Pismen [7]). These approaches have been used exclusively for dynamic analysis by estimating the friction force as a product of the friction coefficient and the velocity of the contact line. Little is known about the static contact line friction just prior to initiation of TCL motion. Nevertheless, since liquid droplets, unlike solid objects, undergo significant topological changes in response to external forces, it is possible to estimate the force necessary to initiate motion of TCL by examining the topological observables (local radius meniscus curvature, local contact angle, etc.) at the critical inclination angle. The dynamics of the static force balance at the TCL have been investigated and the three regimes (gravity dominated, intermediate and surface force dominated) have been identified as shown in Figure 1 (Kim and Kaviany [8]). It was found that the critical inclination angle at an applied potential follows the constant Bo line which suggests that the electrostatic force reduces the contribution of the surface forces. Here, we review the physics behind condensate purge using electrowetting. Using this physical understanding, electrowetting technique is applied to enhance the drainage rate of a prototype heat exchanger. Furthermore, ideal implementation concepts are presented for future reference.

We are thankful for useful discussions with Hailing Wu, Michael Heidenreich and Steve Wayne of Advanced Heat Transfer LLC, and Jeffrey Bainter of Circle Prosco, Inc.

Address correspondence to Professor Massoud Kaviany, Department of Mechanical Engineering, University of Michigan, Ann Arbor, Michigan 48109-2125. E-mail: kaviany@umich.edu

THEORETICAL ANALYSIS

Fundamentals of Surface Forces

Liquids form a spherical cap with a well-defined equilibrium contact angle $\theta_{c,o}$ or spread across the surface as a thin film when condensed or injected onto a solid surface. The precise equilibrium that determines the topology of a droplet is the balance between the liquid–gas σ_{lg}, solid–liquid σ_{sl}, and gas–solid

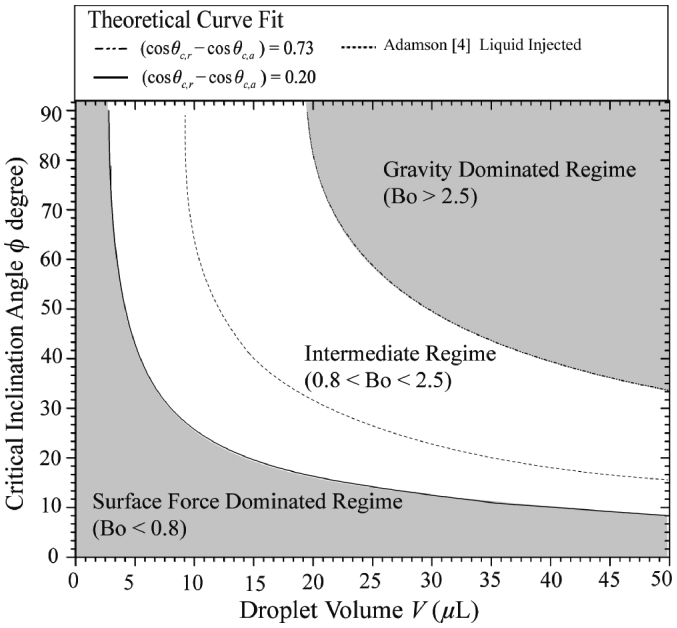

Figure 1 The critical inclination angle with respect to droplet volume for three regimes (gravity dominated, intermediate and surface force dominated). The theoretical curve fit of the experimental results are presented along with data from [4].

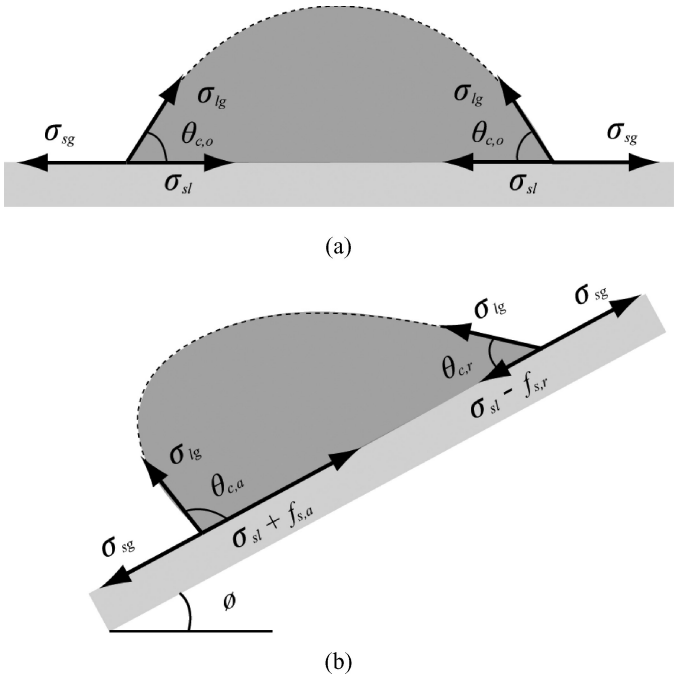

Figure 2 Balance of forces at the TCL for (a) $\varphi = 0^\circ$ and (b) $\varphi > 0^\circ$.

σ_{gs} interfacial tensions. This balance of forces is represented by the free energy at the contact line

$$F_{if} = \sum A_i \sigma_i - \lambda V \tag{1}$$

where λ is the Lagrangian multiplier for the constant volume constraint, A is area, V is the liquid volume and λ is equal to the capillary pressure Δp across the liquid-gas interface. Minimization of the free energy leads the following two conditions which govern the topology (meniscus) of droplet (Adamson [4] and Israelachvili [9]). The first is the meniscus Laplace equation which states that Δp is constant over the entire interface

$$\Delta p = \sigma_{lg}\left(\frac{1}{r_1} + \frac{1}{r_2}\right) \tag{2}$$

where r_1 and r_2 are the two principal radii of curvature of the meniscus. The Laplace equation shows that for homogeneous substrates, liquid droplets adopt a spherical cap shape in mechanical equilibrium. The other is the contact line Young equation

$$\cos\theta_{c,o} = \frac{\sigma_{sg} - \sigma_{sl}}{\sigma_{lg}} \tag{3}$$

This relates the interfacial tension to the apparent contact angle $\theta_{c,o}$. Figure 2a shows the contact angle and the surface tension in equilibrium for liquid droplet on a horizontal surface. For the relevant scale, often, it is possible to adopt a one-dimensional model of the contact line, where the three interfacial tensions are pulling on TCL. For a liquid on an inclined surface, the ratio of the surface forces to gravity is represented by the Bond number ($\mathrm{Bo} = \rho g D^2 \sin\varphi/\sigma_{lg}$), where ρ is the density of the liquid, g is the gravitational constant and D is the droplet diameter. We consider moderate Bond numbers (Bo = 0.8–2.5), so the droplet motion is moderately influenced by gravity. For a plate inclination angle φ, the mass center of the droplet shifts towards the advancing side, giving rise to the local capillary pressure Δp at the liquid–gas interface. The opposite phenomenon exits on the receding side. TCL of the advancing side is pinned due to the contact line friction and is not allowed to advance until a critical inclination angle is reached. Then at the advancing side, according to Eq. (2), reduction in the radius of curvature occurs and causes the contact angle to increase. At the receding side, reduction of the local capillary Δp requires a larger radius of curvature and this results in a smaller contact angle. This difference between the advancing and receding contact angles is referred to as the contact angle hysteresis and is shown in Figure 2b. As seen in the figure, the force balance at the TCL is modified due to the presence of contact line friction. From the point of surface tension equilibrium at the TCL, the contact angle hysteresis can be modeled as the addition of friction, f_s (per unit length), to the σ_{sl} at the advancing side and subtraction of friction, f_s, at the receding side. The radial component of f_s varies along the azimuthal angle ζ, thus, the contact angle varies from $\theta_{c,a,max}$ to $\theta_{c,o}$ then to $\theta_{c,r,min}$. The contact angle hysteresis and the retention force (the sum of f_s over the entire contact line) can be related using following equation for circular droplets,

$$F_s = k\sigma_{lg} R(\cos\theta_{c,r} - \cos\theta_{c,a}) \tag{4}$$

where k is a constant, R is the length scale representing the size of the meniscus, and $\theta_{c,r}$ and $\theta_{c,a}$ are the receding and advancing contact angles. Here k depends on the topology of the droplet and is found empirically using the measured receding

and advancing contact angles at the critical inclination angle. Knowing k and using the droplet force balance, the critical inclination angle can be found. Elsherbini and Jacobi [10, 11] have performed a comprehensive empirical analysis of droplets on aluminum substrates, with commercially available coatings. They propose an empirical relation between the Bond number and the ratio of the receding and advancing contact angles, i.e.,

$$\frac{\theta_{c,a}}{\theta_{c,r}} = 0.01\mathrm{Bo}^2 - 0.155\mathrm{Bo} + 0.97 \tag{5}$$

This relationship is used to estimate the retention force over the entire range of Bond numbers.

Electrowetting

Extensive electrowetting studies have been done with spatial dimensions where gravity effects are negligible (Bond number tending to zero) in the areas such as microfluidics or microelectronics (Berge and Peseux [12], Srinivasan et al. [13], and Yun et al. [14]). Figure 3 renders the contact angles affected by electrowetting. To relate the applied voltage to the change in the effective surface tension, the thermodynamic-electrochemical, energy minimization, and electromechanical approach have been used (Berge [15], Jones [16], and Jones [17]. All of these approaches converge to a single well-accepted electrowetting relation which is presented subsequently. Here the electromechanical approach is reviewed which was first introduced by Jones [16] and starts from the Korteweg-Helmholtz body force density (Landau and Lifschitz [18])

$$\boldsymbol{F}_k = \rho_f \boldsymbol{E} - \frac{\varepsilon_0}{2} E^2 \nabla\varepsilon + \nabla\left[\frac{\varepsilon_0}{2} E^2 \frac{\partial\varepsilon}{\partial\rho}\rho\right] \tag{6}$$

where $\boldsymbol{E}$ is the electric field vector, ρ_f is the fluid charge density, ρ and ε are the mass density and the dielectric constant of the liquid. The last term in Eq. (6) describes the electrostriction and can be neglected. If we assume that the liquid is perfectly conductive, integrating Eq. (6) over the entire volume is equivalent to integrating the Maxwell stress tensor over the liquid-gas interface

$$F_e = \oint T \bullet n\, ds \tag{7}$$

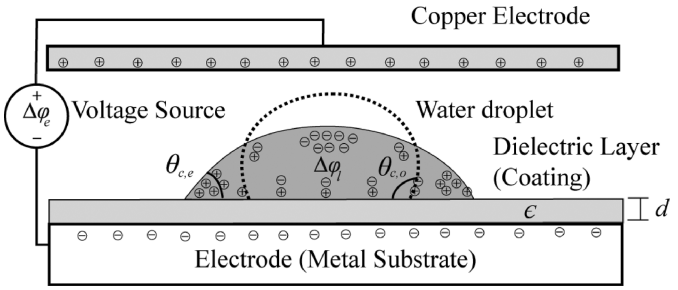

Figure 3 Rendering of electrowetting of the surface droplet on a dielectric coated substrate. The net charge distribution is also shown.

where, $\boldsymbol{T}$ is the Maxwell stress tensor which is written as

$$\boldsymbol{T}_{ik} = \varepsilon_0\varepsilon\left(-\frac{1}{2}\delta_{ik}|\boldsymbol{E}|^2 + \boldsymbol{E}_i\boldsymbol{E}_k\right) \tag{8}$$

where δ_{ik} is the Kronecker delta and $\boldsymbol{n}$ is the normal direction. The tangential component of the electric field at the surface vanishes and the normal component is related to the local surface charge density through $\rho_s = \varepsilon_o\,\varepsilon\, E \bullet \boldsymbol{n}$. Now noting that every term except the component directed along the outward surface normal vanishes, Eq. (7) becomes

$$\boldsymbol{F}_e = \oint \frac{1}{2}\rho_s \boldsymbol{E}\, ds \tag{9}$$

The field and charge distribution are found by solving the electrical Laplace equation for the electrostatic potential with the appropriate boundary conditions. Both the field and charge distributions diverge upon approaching the contact line [19]. Therefore, the Maxwell stress is maximum at the contact line and exponentially decays with distance from the contact line. After integration using $\Delta\varphi = -\mathbf{E} \bullet \boldsymbol{n}$ ds, where $\Delta\varphi$ is the voltage drop across the interface, the horizontal component of the Maxwell stress is

$$f_e = \frac{\varepsilon_o\varepsilon}{2d}\Delta\varphi^2 \tag{10}$$

Since this force acts only on the contact line and is perpendicular to TCL, it is used in the force balance and the Young equation, i.e.,

$$\sigma_{sl,e}^{\mathrm{eff}} = \sigma_{sl} - \frac{\varepsilon_0\varepsilon}{2d}\Delta\varphi^2 \tag{11}$$

$$\cos\theta_{c,e} = \cos\theta_{c,o} + \frac{\varepsilon_0\varepsilon}{2\sigma_{lg}d}\Delta\varphi^2 \tag{12}$$

where $\theta_{c,e}$ is the electrowetted contact angle, $\theta_{c,o}$ is the neutral contact angle, ε is the dielectric constant of the dielectric layer underneath the water droplet, d is the thickness of the dielectric layer, and $\Delta\varphi$ is the applied potential between the liquid and the electrode underneath the dielectric layer. Ideally, as the potential is increased, the electrowetted contact angle approaches zero. However, it is found that the contact angle saturates at a value $\theta_{c,sat}$ varying between 30° and 80°, depending on the system (Moon et al. [20] and Peykov et al. [21]). This contact angle saturation can be explained as an electron-discharge mechanism, together with the vertical component of the electrostatic force acting on the contact line (Kang [22]).

Physics of Droplet Purge Initiation

Physics of the electrowetting assisted purge of droplets can be analyzed using a simple force balance at TCL. At TCL, a force of per unit length is applied in the radial direction as predicted by Eq. (10). As a result, the x component of the electrowetting force will vary as the cosine of the azimuthal angle ζ. In contrast, the contact line friction is constant along TCL in the x direction, since it is assumed that the friction is a reaction force existing only in the x direction and that droplet weight is uniformly distributed at liquid–solid interface. Note that the integral of the contact line friction at the critical inclination angle is equal to the retention force, which is given by Eq. (4). By curve fitting the data points under no electrowetting conditions, the magnitude of k from the experiment was found to be 1.845. Then according to the classical droplet mechanics and by using the retention force data, the sum of the forces at the critical inclination angle can be written as

$$F_x = \int_{-\frac{\pi}{2}}^{\frac{\pi}{2}} 2Rf_e \cos\zeta d\zeta - \frac{1}{2}F_{sx}$$

$$= \int_{-\frac{\pi}{2}}^{\frac{\pi}{2}} R\frac{\varepsilon_o \varepsilon}{d}\Delta\varphi^2 \cos\zeta d\zeta - 0.923\sigma_{\mathrm{lg}} R(\cos\theta_{c,r} - \cos\theta_{c,a}) \tag{13}$$

We have assumed that the applied forces are concentrated at TCL, as graphically represented in Figure 4. From the figure we see that the contact line of the advancing side will start to slip when the electrowetting overcomes the local static contact line friction value at the location of $\theta_{c,a,max}$. As f_e becomes larger with increase in potential, the portion of the contact line which begins to slip increases. Also, as the contact line begins to slip, it causes an instantaneous reduction in the advancing contact angle. When the advancing contact angle is reduced, according to Eq. (12), the retention force is reduced which results in lowering of the critical inclination angle (for given liquid volume). When a sufficient portion of the contact line friction is removed, the bulk liquid motion is initiated. In sum, the sequence of liquid motion under electrowetting can be described as first, at the onset of motion, the droplet is charged and experiences electrowetting which overcomes the static TCL friction. When the sum of the gravity and electrowetting force is larger than the static friction over the entire contact line of the droplet, the bulk condensate motion is initiated. As the droplet advances, the electrostatic energy is dissipated and dewetting becomes apparent. When the droplet recovers its original topology, it experiences a rise in electrostatic energy due to its proximity to the over-hanging electrode and this sequence is repeated. Using the preceding droplet physics, prediction of the electrowetting reduction of the critical inclination angle is possible by using a simple force balance at the TCL. The observation indicates minimum or no advancing of receding contact line until the advancing contact line has well advanced, thus, it is reasonable to assume that the dominant criteria for the initiation of the droplet motion is the force balance at the advancing contact line (Kim [8]). As long as the droplet is not separated, this treatment of the force on the contact line is valid. The retention force can be estimated using Eq. (4) with the empirical contact angle relation (5). The electrowetting force can be calculated by integrating the x component acting on TCL over the azimuthal angle for the advancing portion of the droplet. Then by solving for the inclination angle which the gravity balances, the resultant of the retention force and the electrowetting force, it is possible to obtain a theoretical prediction of the variation of the critical inclination angle with the applied potential. This angle is found by solving the following equation

$$\phi = \sin^{-1}\left(\frac{\int_{-\frac{\pi}{2}}^{\frac{\pi}{2}} R\frac{\varepsilon_o \varepsilon}{d}\Delta\varphi^2 \cos\zeta d\zeta - 0.923\sigma_{lg}(\cos\theta_{c,a} - \cos\theta_{c,r})}{\rho g V}\right) \tag{14}$$

Note the underlying assumptions that friction force at the rear TCL does not contribute to the initiation of the droplet motion and that the weight of the droplet is applied to the front half of the droplet.

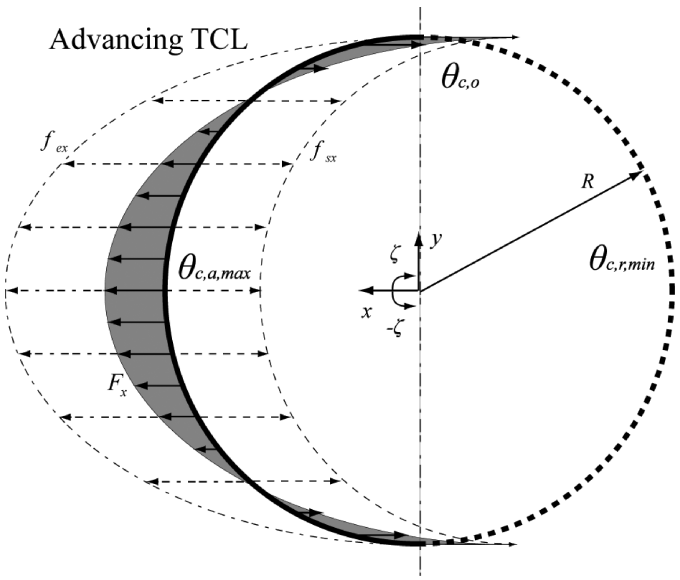

Figure 4 Graphical representation of balance between the retention and electrowetting forces, at the advancing TCL.

EXPERIMENTAL ANALYSIS

Implementation of Electrowetting in Heat Exchangers

The theoretical analyses in the preceding sections have indicated that by using electrowetting droplet motion initiation at

low Bond numbers is possible. This would significantly increase the drainage rate in heat exchangers. To extend the theoretical prediction to practical application, a series of experiments were designed and performed. Figure 5 presents a detailed picture of an electrowetting assisted droplet purge in prototype heat exchangers manufactured by AHT (Advanced Heat Transfer). The heat exchangers were coated with a dielectric layer (polymer based electric insulation coating $\varepsilon = 2.4$ and $\theta_{c,o} = 70^\circ$) with 200 μm in thickness. A second polymer-based P4 ($\varepsilon = 3.0$ and $\theta_{c,o} = 110^\circ$) hydrophobic coating (Circle Prosco, Bloomington, IN, USA) with 300 μm in thickness was coated on top of the first layer. Subsequently, horizontal and vertical copper electrodes where installed between the fins of the heat exchangers via external acrylic frame. Then the heat exchangers were connected to a refrigeration unit and were operated under 80% humidity condition for 60 min. The heat exchanger surface temperature T_{HX} was measured to be 0.2°C. When condensation began to form, electric potential of 600 V was applied. The experiment was photographed using a DSLR camera with a 1:1 macrolens. The figure shows that there exists clear contrast between the fins which have been subjected to electrowetting forces and the ones which were not. The droplets which were formed under heat exchanger operations have either been purged or on the verge of purge for the fins which have electrodes, whereas significant droplet retention is observed on the fins which do not have electrodes. Figure 6 shows the drainage rate (mass of water drained per unit time) normalized with respect to base (no coat) heat exchanger of different passive and active surface treatments. The data show approximately 150% improvement in drainage rate compared to heat exchanger with no coat. Also, for manual target excitation (where electrodes were manually brought in proximity to the droplets), there was approximately 290% increase in the drainage rate showing significantly improved drainage potential when optimization is achieved. In light of previously shown potential-improvement of drainage rate in heat exchangers, we present a ideal conceptual design in which the electrowetting assisted drainage can be implemented in a full scale heat exchanger. Figure 7 shows one of the optimized implementations of electrowetting technique in heat exchangers. The heat exchanger is coated with a hydrophobic dielectric coating and the electrodes are suspended between the fins via external frame. The electrodes are vertically oriented to minimize the blockage of liquid droplets. Although there

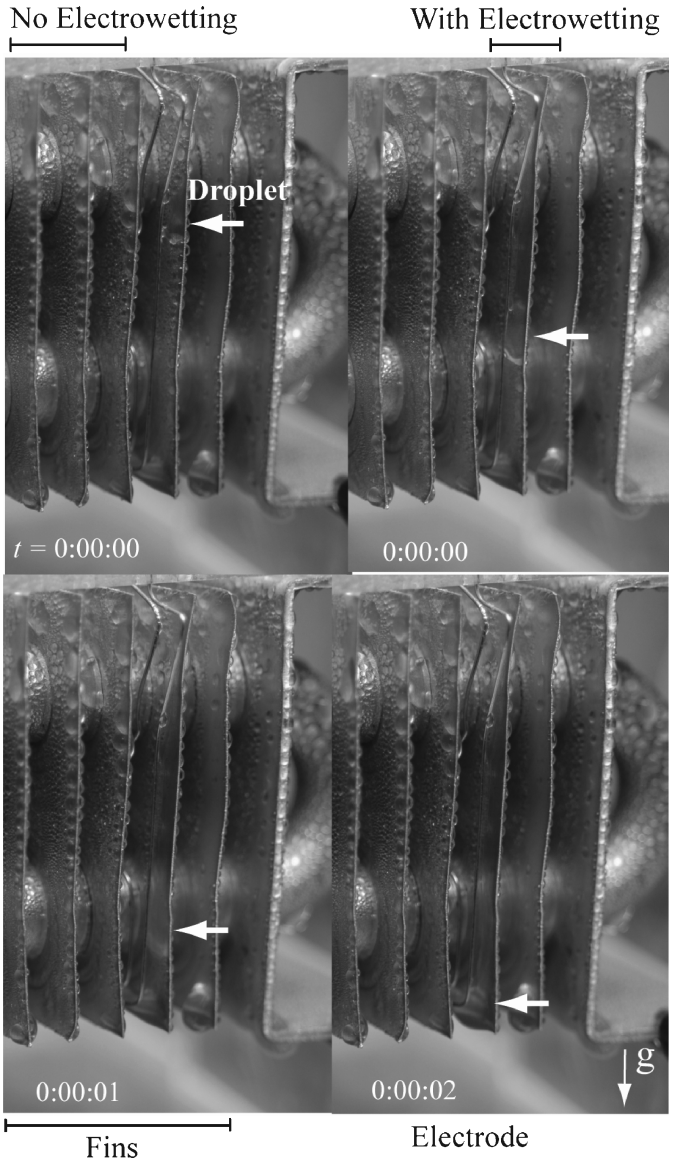

Figure 5 Image of initiation of droplet purge using electrowetting using vertical electrodes, for different elapsed times. The environmental conditions are $T_{HX} = 0.2^\circ$C, relative humidity = 80% and exposed time duration of 60 mins. The location of the droplet is indicated using arrows. Note the contrast between fins with and without electrowetting.

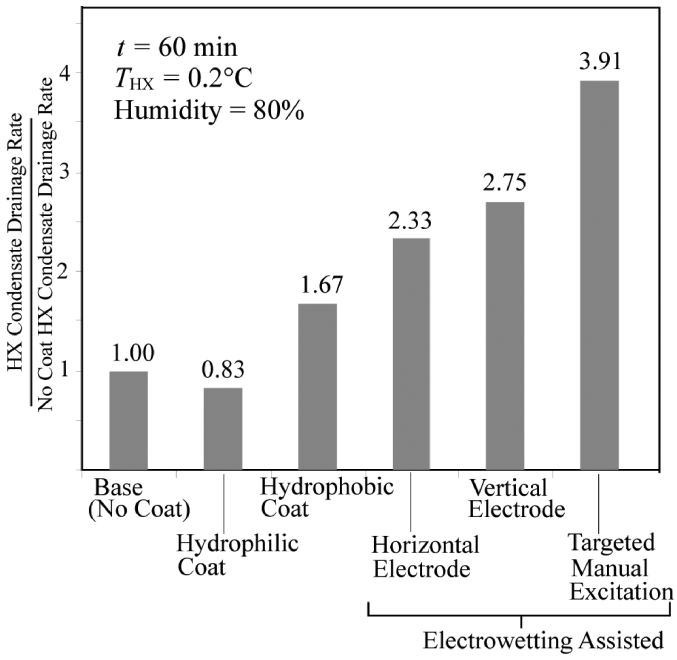

Figure 6 Drainage rate for prototype heat exchangers with different passive and active droplet-retention prevention methods. The drainage rates have been normalized with respect to base (no coat) heat exchanger.

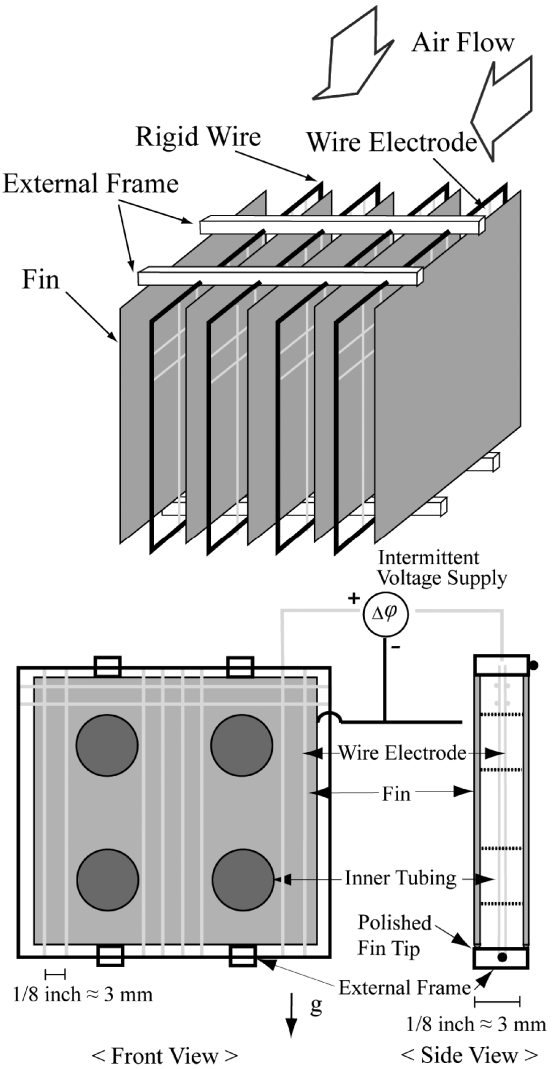

Figure 7 Conceptual rendering of one of the optimized electrode designs which utilizes electrowetting as an active means of purging of droplets.

still exist many challenges in electric isolation and current lack of high performance coating, in the future, we expect that these kinds of electrowetting assisted drainage in heat exchangers will significantly reduce the water retention rate thereby improving the heat exchanger performance by many folds.

CONCLUSION

Electrowetting purged surface condensate in evaporators has been investigated using physics of the force balance at the three-phase contact line. Using a prototype heat exchanger, the theory was applied to investigate the improvement of drainage under electrowetting conditions. Significant improvements—up to 290% increase in the drainage rate—were observed paving the way to a full scale implementation of physics using elecrowetting as the means of condensate purge. Based on the theoretical insight and the preliminary experimental investigation, we propose an electrode-heat exchanger design which will enhance the current performance of the evaporator. By using the new electrowetting implemented heat exchanger design and overcoming the following challenges: need for enhanced electrical insulation, high performance dielectric coating and polished find tip, it is expected that the evaporator performance will increase by many folds.

NOMENCLATURE

A	area, m^2
Bo	bond number
D	diameter, m
$\boldsymbol{E}$	electric field strength, V/m
$\boldsymbol{F}_{if}$	total force, N
f_s	friction force, N
g	gravitational acceleration, $m.s^{-2}$
k	retention force constant
$\boldsymbol{n}$	unit vector
Δp	pressure drop, Pa
R	droplet radius, m
r_1	minuscule radius, m
$\boldsymbol{T}$	Maxwell stress tensor, Pa
T_{HX}	Temperature, °C
V	Volume, m^3

Greek Symbols

δ_{ik}	Kronecker delta
ζ	azimuthal angle, °
θ_c	contact angle, °
λ	Lagrange multiplier
ρ	mass density, kg/m^3
ρ_f	liquid charge density, C/m^3
ρ_s	surface charge density, C/m^3
σ_{ij}	$i - j$ interfacial tension, N/m

Subscripts

c,a	advancing contact angle
c,e	electrowetted contact angle
c,o	equilibrium contact angle
c,r	receding contact angle
g	gas
HX	heat exchanger
if	interface
l	liquid
max	maximum
min	minimum
s	static or solid

REFERENCES

[1] Emery, A. F., and Siegel, B. L., Experimental Measurements of the Effects of Frost Formation on Heat Exchanger Performance, In *Proceedings of AIAA/ASME Thermophysics and Heat Transfer Conference, Heat and Mass Transfer in Frost and Ice packed Beds and Environmental Discharges*, pp. 1–7, 1990.

[2] Na, B., and Webb, R. L., New Model for Frost Growth Rate, *International Journal of Heat Mass Transfer*, vol. 47, no. 5, pp. 925–936, 2004.

[3] Ren, H., Fair, R. B., Pollack, M. G., and Shaughnessy, E. J., Dynamics of Electro-Wetting Droplet Transport, *Sensors and Actuators B*, vol. 87, pp. 201–206, 2002.

[4] Adamson, A., *Physical Chemistry of Surfaces*, 4th edition, Wiley, New York, 1982.

[5] deGennes, P. G., On Fluid/Wall Slippage, *Langmuir*, vol. 18, pp. 3413–3414, 2002.

[6] Oron, A., Long-Scale Evolution of Thin Liquid Films, *Reviews of Modern Physics*, vol. 69, pp. 931–980, 1997.

[7] Pismen, L. M., Mesoscopic Hydrodynamics of Contact Line Motion, *Colloids and Surfaces A*, vol. 206, pp. 11–30, 2002.

[8] Kim, J., and Kaviany, M., Purging of Dropwise Condensate by Electrowetting, *Journal of Applied Physics* vol. 101, pp. 103520–103527, 2007.

[9] Israelachvili, J. N., *Intermolecular and Surface Forces*, 1st edition, Academic, San Diego, California, 1985.

[10] Elsherbini, A. I., and Jacobi, A. M., Liquid Drops on Vertical and Inclined Surfaces I. An Experimental Study of Drop Geometry, *Journal of Colloid and Interface Science*, vol. 273, pp. 556–565, 2004.

[11] Elsherbini, A. I., and Jacobi, A. M., Liquid Drops on Vertical and Inclined Surfaces ii. A Method for Approximating Drop Shapes, *Journal of Colloid and Interface Sci.*, vol. 273, pp. 566–575, 2004.

[12] Berge, B., and Peseux, J., Variable Focal Lens Controlled by an External Voltage: An Application of Electrowetting, *The European Physical Journal E*, vol. 3, pp. 159–163, 2000.

[13] Srinivasan, V., Pamula, V. K., and Fair, R. B., An Integrated Digital Microfluidic Lab-on-a-Chip for Clinical Diagnostics on Human Physiological Fluids, *Lab on a Chip*, vol. 4, pp. 310–315, 2004.

[14] Yun, K. S., Bu, I. J., Bu, J. U., Kim, C. J., and Yoon, E., A Surface-Tension Driven Micropump for Low-Voltage and Low-Power Operations, *Journal of Microelectromechanical Systems*, vol. 11, pp. 454–461, 2002.

[15] Berge, B., Electrocapillarity and Wetting of Insulator Films by Water, *Comptes Rendus De l'Academie des Science., Series II: Mec., Phys., Chim., Scie.Terre Univers*, vol. 317, pp. 157–163, 1993.

[16] Jones, T. B., On the Relationship of Dielectrophoresis and Electrowetting, *Langmuir*, vol. 18, pp. 4437–4443, 2002.

[17] Jones, T. B., An Electromechanical Interpretation of Electrowetting, *Journal of Micromechanics and Microengineering*, vol. 15, pp. 1184–1187, 2005.

[18] Landau, L. D., and Lifschitz, E. M., *Electrodynamics of Continuous Media*, Pergamon, Oxford, UK, 1960.

[19] Vallet, M., Vallade, M., and Berge, B., Limiting Phenomena for the Spreading of Water on Polymer Films by Electrowetting, *The European Physical Journal B*, vol. 11, pp. 583–591, 1999.

[20] Moon, H., Cho, S. K., Garrell, R. L., and Kim, C. J., Low Voltage Electrowetting-on-Dielectric, *Journal of Applied Physics*, vol. 92, pp. 4080–4087, 2002.

[21] Peykov, V., Quinn, A., and Ralston, J., Electrowetting: A Model for Contact-Angle Saturation, *Colloid and Polymer Science*, vol. 278, pp. 789–793, 2000.

[22] Kang, K. H., How Electrostatic Fields Change Contact Angle in Electrowetting, *Langmuir*, vol. 18, pp. 10318–10322, 2002.

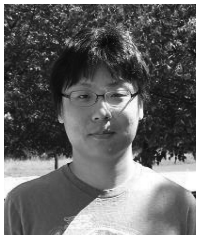

Jedo Kim is a Ph.D. student at the Heat Transfer Physics lab, Department of Mechanical Engineering, University of Michigan, Ann Arbor. He received his M.S. from University of Michigan and his B.S. from University of Toronto (2004). Currently, he is working in atomic-level heat regeneration using anti-Stokes luminescence.

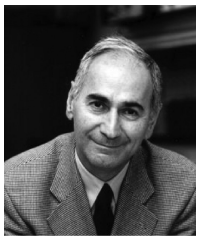

Massoud Kaviany is Professor of Mechanical Engineering and Applied Physics at University of Michigan, since 1986. His Ph.D. is from University of California-Berkeley. His education-research field is heat transfer physics.